Numerical and experimental study of the redistribution of energetic and impurity ions by sawteeth in ASDEX Upgrade

F. Jaulmes[1], B. Geiger[2], T. Odstrčil[2], M. Weiland[2], M. Salewski[3], A.S. Jacobsen[3], J. Rasmussen[3], M. Stejner[3], S.K. Nielsen[3], E. Westerhof[1], the EUROfusion MST1 Team[4] and the ASDEX Upgrade team[2]

[1] FOM Institute DIFFER, Eindhoven, The Netherlands
[2] Max-Planck-IPP, Boltzmannstr. 2, 85748 Garching, Germany
[3] DTU, Department of Physics, Dk-2800 Kgs. Lyngby, Denmark
[4] See http://www.euro-fusionscipub.org/mst1

E-mail: F.Jaulmes@differ.nl

Abstract. In the non-linear phase of a sawtooth, the complete reconnection of field lines around the $q = 1$ flux surface often occurs resulting in a radial displacement of the plasma core. A complete time-dependent electromagnetic model of this type of reconnection has been developed and implemented in the EBdyna_go code. This contribution aims at studying the behaviour of ions, both impurity and fast particles, in the pattern of reconnecting field lines during sawtoothing plasma experiments in the ASDEX Upgrade tokamak by using the newly developed numerical framework. The simulation of full reconnection with tungsten impurity that include the centrifugal force are achieved and recover the Soft X-Ray (SXR) measurements. Based on this full-reconnection description of the sawtooth, a simple tool dedicated to estimate the duration of the reconnection is introduced. This work then studies the redistribution of fast ions during several experimentally observed sawteeth. In some cases of sawteeth at ASDEX Upgrade, full reconnection is not always observed or expected so the code gives an upper estimate of the actual experimental redistribution. The results of detailed simulations of the crashes are compared with measurements from various diagnostics such as Collective Thomson Scattering (CTS) and Fast-Ion D-Alpha (FIDA) spectroscopy, including FIDA tomography. A convincing qualitative agreement is found in different parts of velocity space.

1. Introduction

A sawtooth crash is triggered when the $m = 1$ mode is destabilized [1], where m is a poloidal mode number. We have built a numerical model named EBdyna_go [2] (or EBdyna for conciseness) of the sawtooth collapse based on the original full reconnection pattern suggested by Kadomtsev [3] with the dynamical evolution of the electromagnetic fields during the collapse as introduced by Kolesnichenko et al. in [4]. The code evolves

the ions according to their momentum equation. The first part of the sawtooth collapse is the 'crash' phase where reconnection occurs. The second part is the 'reorganization' phase where axi-symmetry of the field line topology is recovered. EBdyna is applied here in the specific experimental configuration of the ASDEX Upgrade tokamak to understand the effect of the collapse on ions with different orbit categories (passing or trapped) and with a large range of velocities (from thermal impurity ions up to Neutral Beam Injection (NBI) generated 60 keV fast ions).

The experimental conditions and the model for the dynamical evolution of the electromagnetic field during a sawtooth collapse are discussed in Section 2. An analysis of the effect of the reconnection on tungsten impurity ions is given in section 3. The numerical modelling is then applied in section 4 to a population representative of a 60 keV NBI system (line Q3 in ASDEX Upgrade), as obtained by the NUBEAM-TRANSP solver [5]. We compare CTS [6] and FIDA [7] measurements with the EBdyna simulations. Finally, Section 5 comments on the various dynamical behaviour of the NBI ions depending on their energy and pitch, as well as their orbit width and angular helical precession.

2. Dynamical modelling of the sawtooth collapse in ASDEX Upgrade

2.1. Experimental plasma conditions

The experiments that we consider in this paper include a significant population of fast particles from the co-current NBI system, representing up to one third of the bulk pressure. These particles affect the stability of the plasma [8], yielding a sawtooth cycle with large sawteeth where the radial size of the mixing region r_{mix} extends up to half of the minor radius $a \simeq 0.51$m. The major radius of the torus is $R_0 \simeq 1.63$m in the equilibrium as reconstructed by the solver FINESSE [9]. This solver allows in particular to obtain a representation of the magnetic field in straight-field line coordinates. On a given flux surface, the safety factor $q = \mathrm{d}\varphi/\mathrm{d}\theta$ describes the helicity of the field line (θ being a poloidal angle and φ being the toroidal angle). In table 1 we give values of the plasma parameters (or their average) at the pre-crash position of the $q = 1$ flux surface (subscript 1). The subscript 0 refers to the on-axis value. The calculation of the approximate value of the ideal growth rate γ_I of the $m = 1$ mode was done according to the energy principle (considering the change of potential energy δW_{MHD} related to a small displacement ξ), using results from [10] and taking into account the trapped particle damping γ_{tr} [11] as well as the adiabatic damping γ_{f} due to the NBI fast particles [8]. The resulting ideal growth rate is then expressed as:

$$\begin{aligned}
\gamma_I =& \gamma_{\mathrm{MHD}} + \gamma_{\mathrm{tr}} + \gamma_{\mathrm{f}} \\
\gamma_{\mathrm{MHD}} =& -\frac{v_{A1}}{R_0}\left(\frac{r_1}{R_0}\right)^2 \frac{\sqrt{3}\pi}{s_1}\delta\hat{W}_{\mathrm{MHD}} \\
\delta\hat{W}_{\mathrm{MHD}} =& \frac{R_0^3\mu_0}{6\pi^2 B_0^2|\xi|^2 r_1^4}\delta W_{\mathrm{MHD}} = -(1-q_0)\left[3\left(1-\frac{r_1}{r_2}\right)\beta_{P1}^2 - \frac{13}{112}\right]
\end{aligned} \tag{1}$$

where v_{A1} is the Alfvén velocity at $q = 1$ (at approximate radial position $r = r_1$) and $\beta_{P1} = \left(2\mu_0 \int_0^{r_1} \left(\frac{r}{r_1}\right)^2 \left(-\frac{\mathrm{d}P}{\mathrm{d}r}\right) \mathrm{d}r\right) / B_{\theta 1}^2$ ($B_{\theta 1}$ being the poloidal magnetic field).

In order to write a model dispersion relation for the $m = 1$ instability, we introduce the small resistive dissipative term for a given parallel resistivity $\eta_\parallel$:

$$\epsilon_\eta = \frac{\eta_\parallel}{\mu_0 r_1^2 \hat{\omega}_A} \text{ with } \hat{\omega}_A = \frac{v_{A1} s_1}{\sqrt{3} R_0} \tag{2}$$

where $\hat{\omega}_A$ is an Alfvén frequency at the resonance surface and $s_1 = r_1(\mathrm{d}q/\mathrm{d}r)_{r=r_1}$ the magnetic shear at $q = 1$; $\mu_0 = 4\pi \times 10^{-7}$ TmA^{-1} is the permeability of free space. Without diamagnetic corrections (damping) due to the finite size of the Larmor orbit ρ_{Li}, the $m = 1$ resistive mode growth rate in the large Larmor radius resistive limit is [12]:

$$\gamma_{\eta 0} = \hat{\omega}_A \left(\frac{\rho_{Li}}{r_1}\right)^{4/7} \left(\frac{2(1 + T_e/T_i)}{\pi}\right)^{2/7} \epsilon_\eta^{1/7} \ . \tag{3}$$

A more realistic picture should include the diamagnetic effects related mostly to the diamagnetic frequency at $q = 1$, $\omega_{*i} = \frac{1}{n_{i1} r_1 e B} \frac{\mathrm{d}P_i}{\mathrm{d}r}$ and that can be included by using the dispersion relation [13] :

$$\gamma^{1/2}(\gamma - i\omega_{*i})^{1/2}(\gamma - i\omega_{ne})^{3/2}(\gamma - i\omega_{ni}) = \hat{\omega}_A^{7/2} \frac{2(1 + T_e/T_i)\rho_s^2}{\pi r_1^2} \epsilon_\eta^{1/2} \tag{4}$$

which we have solved for the real part and documented in table 1 as γ_η. The ion and electron drift frequencies have been introduced and are defined as:

$$\omega_{ni} = \frac{T_i}{e B_1 n_i r_1} \frac{\mathrm{d}n_i}{\mathrm{d}r} \quad \text{and} \quad \omega_{ne} = -\frac{T_e}{e B_1 n_e r_1} \frac{\mathrm{d}n_e}{\mathrm{d}r} \quad . \tag{5}$$

The value of γ_η is to be compared with the ideal one in the case of large ideal growth rate $\gamma_I > |\omega_{*i}|$: under this condition, when also $\gamma_I > \gamma_\eta$, the precursor is likely ideal in nature. Otherwise, when $|\gamma_I|$ is small compared with $|\omega_{*i}|$, the precursor can be resistive (or more generally dissipative) in nature as described by equation (4): this version of the $m = 1$ internal kink mode is found to be unstable in all cases. The case $\gamma_I < -|\omega_{*i}|$ corresponds to the drift-tearing mode. In the table 1, sawtooth A might be in ideal regime, whereas sawteeth C and E are possibly in drift-tearing regime.

2.2. Pre-collapse equilibrium and coordinates

The total pressure profile and the safety factor profile were obtained from TRANSP. The equilibrium code FINESSE [14] was then used to reproduce these data. The simulations were performed with a current in the opposite direction as that of the toroidal magnetic field, as in the experiments. The unit vectors obey $\mathbf{e}_{\boldsymbol{\varphi}} = \mathbf{e}_{\mathbf{R}} \times \mathbf{e}_{\mathbf{Z}}$: this results in a positive toroidal field component and a negative current (figure 1, where the direction of the toroidal field $\mathbf{e}_{\boldsymbol{\varphi}}$ is pointing out of the figure). The output of the equilibrium code gives us a mesh in the poloidal plane representative of the poloidal flux contours

Table 1. Comparison of the experimental parameters just before the considered sawteeth. The global plasma current was $I_p \simeq 1$MA and the position of the magnetic axis was approximately at $R_{axis} \simeq 1.68$m. Successively listed are: the poloidal beta β_{p1}, on-axis safety factor q_0 ,toroidal rotation Ω_1 , radial position of $q = 1$, electron temperature T_{e1}, ion temperature T_{i1}, electron density n_{e1}, Larmor radius ρ_{Li1}, electron skin depth d_{e1}, helical flux $|\psi_{*1}|$, ideal growth rate γ_I, diamagnetic angular frequency $|\omega_{*i}|$ and reconnection durations (experimental and modelling), dissipative growth rate $\gamma_{\eta 0}$ without damping, γ_η with diamagnetic damping. τ_{cr} refers to the duration of the reconnection phase of the sawtooth. The 'exp' label stands for the experimental value and 'reco' stands for the value obtained from solving expression (8). The experimental value from SXR signals was not available in case C.

	A	B	C	D	E
parameter	#30382@2.3s	#30382@2.5s	#32324@2.46s	#30815@2.97s	#31557@2.25s
β_{p1}	0.37	0.38	0.415	0.44	0.257
q_0	0.65	0.82	0.96	0.86	0.962
Ω_1 (krad/s)	33	45	66	47	70
r_1 (m)	0.21	0.2	0.21	0.17	0.22
T_{e1} (keV)	2.2	2.4	3.0	2.3	2.4
T_{i1} (keV)	1.7	2.8	2.4	3.3	2.0
n_{e1} (10^{19}m^{-3})	2.4	3.5	3.6	3.9	2.85
ρ_{Li1} (mm)	2.2	2.8	2.6	3.2	2.5
d_{e1} (mm)	1.1	0.91	0.88	0.85	1.0
$\lvert\psi_{*1}\rvert$ (2πTm^2)	0.0115	0.0054	0.0016	0.0031	0.002
γ_I (s^{-1})	2.5 10^4	-0.19 10^4	-8.5 10^4	-0.38 10^4	-8 10^4
$\lvert\omega_{*i}\rvert$ (rad/s)	1.71 10^4	1.8 10^4	2.2 10^4	3.66 10^4	1.8 10^4
$\gamma_{\eta 0}$ (s^{-1})	2.0 10^4	1.2 10^4	5.1 10^3	1.0 10^4	6.2 10^3
γ_η (s^{-1})	1.9 10^4	1.0 10^4	1.95 10^3	0.9 10^3	2.85 10^3
τ_{cr} exp (μs)	~ 90	130	n/a	150	~ 160
τ_{cr} reco (μs)	82	117	200	151	180

and of a straight-field-line poloidal angle. EBdyna matches the pre-crash TRANSP q profile with a precision of about 8%. FINESSE provides the horizontal coordinate $X(\psi, \theta) = R(\psi, \theta) - R_0$ and the vertical one $Z(\psi, \theta)$. Here ψ is the (divided by 2π) poloidal magnetic flux. Regarding the description of the particles, the parallel velocity $v_\parallel$ of co-current circulating particles is thus negative. We define the pitch $\mathcal{P}$ of a passing ion as $\mathcal{P} = -\left\langle v_\parallel \right\rangle / v$ where the average is taken over one bounce-transit orbit and v is the total velocity, assumed approximately conserved. Correspondingly we also define the trapping parameter $\lambda_0 = \mu B_0 / \mathcal{E}_{\text{kin}}$ where μ is the magnetic moment of an ion and $\mathcal{E}_{\text{kin}}$ its kinetic energy.

For convenience, we use a length index r to label flux surfaces. It is defined as $r = \sqrt{\mathcal{S}(\psi)/\pi}$ where $\mathcal{S}(\psi)$ is the area of the surface enclosed by the poloidal contour of the flux surface ψ. We also use the normalized radial flux coordinates

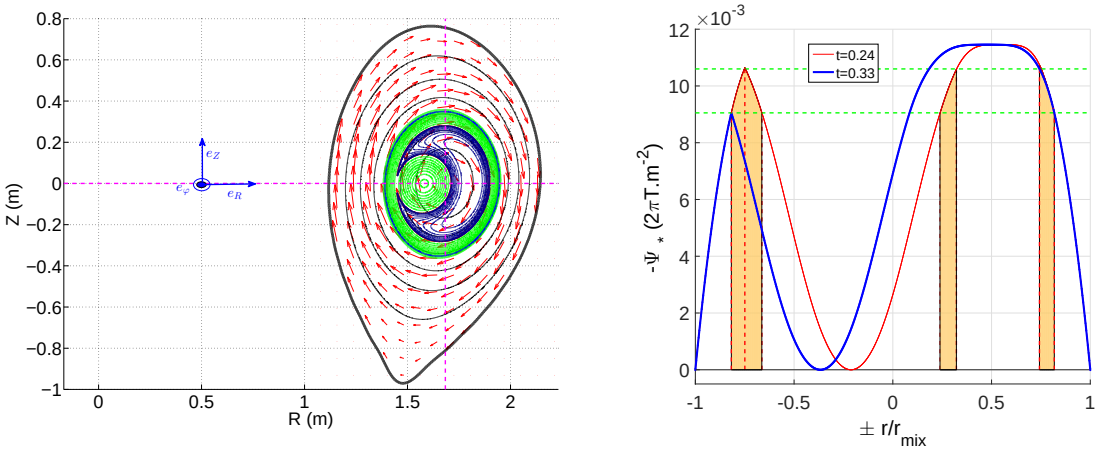

Figure 1. Left: Geometry of the experiment as represented in the simulations with unit vectors $\mathbf{e_\varphi} = \mathbf{e_R} \times \mathbf{e_Z}$. The red arrows represent the intensity and direction of the poloidal field. Right: Values along the horizontal axis (radial direction $\mathbf{e_X}$ at $Z = Z_{\text{axis}}$) of the helical magnetic flux ψ_* compared at two instants during the reconnection (given in the caption as a fraction of the collapse duration τ_{coll}) in the case of sawtooth A. The flux included in the orange regions has contributed to the buildup of the magnetic island as seen on the left figure. The horizontal dashed green lines indicate the values of the flux reconnecting at each time point.

$\rho_{\text{tor}} = \sqrt{\psi_{\text{tor}}/\max(\psi_{\text{tor}})}$, where ψ_{tor} is the toroidal magnetic flux.

2.3. Description of the sawtooth collapse

The global description considered for the reconnection occurring during a sawtooth collapse is designed according to Kadomtsev [3] and as sketched in figure 1. Surfaces that have identical helical flux ψ_* on both sides of the separatrix reconnect during the crash and create a new helical flux surface contour. The helical flux corresponds to an auxiliary helical field $\mathbf{B}_* = (\mathbf{e_\varphi} \times \boldsymbol{\nabla}\psi_*)/R$. The complete description of the evolution of the electromagnetic potentials was described in [4] and implemented in EBdyna [2]. Figure 2 illustrates the contours of the electric potential Φ during the reconnection in the geometry of ASDEX Upgrade.

The crash time that we consider in this study is typically of about $\tau_{cr} \sim 120\mu$s. In table 1, the values are based on the radial position of the maximum of emission as seen in the Soft-X-ray tomography (see figure 3). The total collapse simulation is assumed to last about $\tau_{coll} \sim 250\mu$s. The dynamic is supposed to be close to the one given by the model described in [4] except that we consider that the reconnection phase of duration τ_{cr} represents roughly 48% of τ_{coll} (it is by default about 65% (or exactly $1 - \text{atan}(2)/\pi$) from [4] when the shaping parameter α is increased linearly with time).

In some of the crashes considered (eg. A and E), the impurity density is not peaked yet. In theses cases, a large uncertainty of about 50% remains on the real dynamics of the reconnection. The next section investigates the peculiar behaviour of the maximum

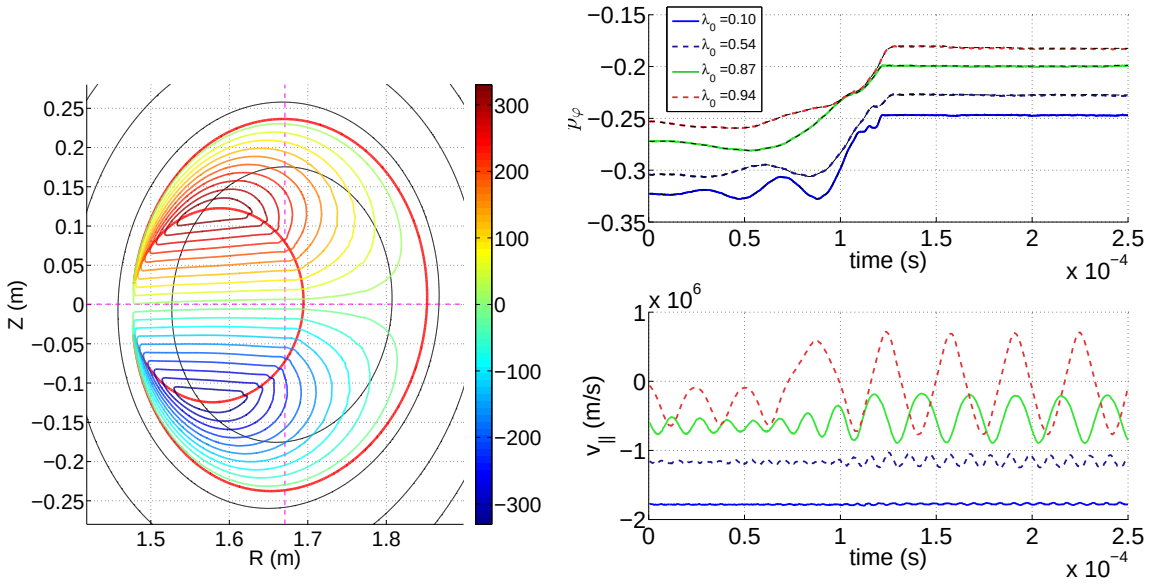

Figure 2. Left: Representation of the contours of the electric potential Φ in V for the sawtooth reconnection of AUG#30815 at 2.97s (case D). The red lines indicate the position of the $m = 1$ island separatrix. Right: compared trajectories of NBI ions of about 33keV during this sawtooth. These particles were initially in the core and are redistributed to the mixing radius region. The change of orbit category of the particle having initially $\lambda_0 = 0.94$ is clearly seen in the bottom figure.

of emission of tungsten due to the high centrifugal force.

3. Comparison of Soft X-Ray tomography with tungsten impurity simulations

3.1. Modifications of the motions of ions to take into account a centrifugal force

In the simulations, an arbitrary steep density profile of tungsten (W) ions having charge $Z_i = 35$ [15] and mass $m = 3.053\ 10^{-25}$kg is specified. This arbitrary profile allows to qualitatively resolve the maximum of density of impurity with a good resolution. The velocity of the tungsten is distributed according to Maxwell-Boltzmann statistics with a temperature equal to that of the background ions. Since the plasmas in the ASDEX Upgrade experiments receive a significant amount of momentum from the NBI particles, they gain a large angular toroidal rotation $\Omega(\psi)$. This rotation has the direction of the toroidal current (negative with our convention). The tungsten population undergoes a significant effect of the plasma rotation that can be described by the centrifugal force in the reference frame of the plasma: $\mathbf{f_c} = mR\Omega^2\mathbf{e_R}$. The effect of the Coriolis force is assumed to be negligible. The momentum equation and the algorithm used to evolve the position are found in [2]. The total electric field $\mathbf{E}$ felt by the particles is implemented

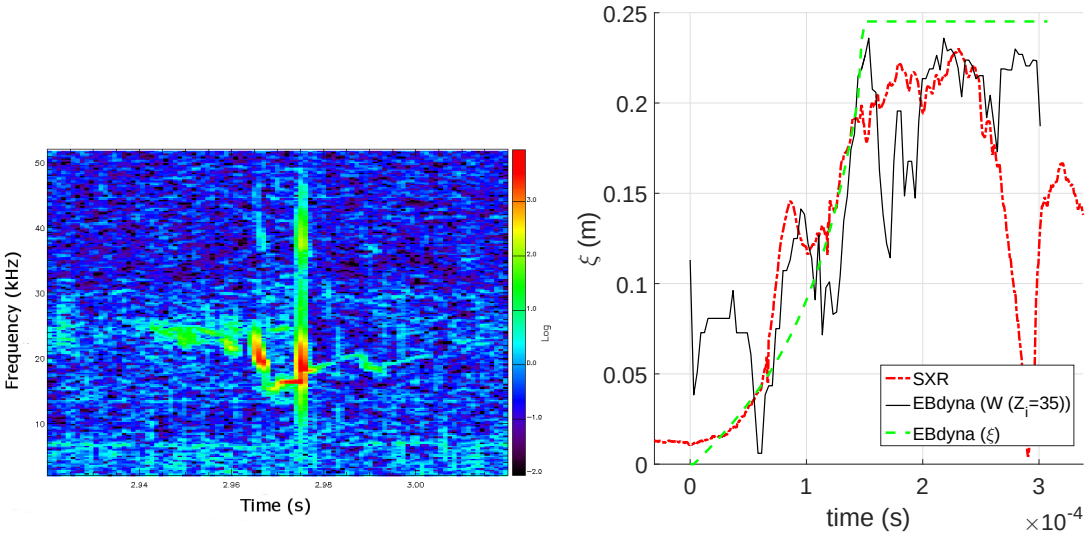

Figure 3. Left: magnetic spectrogram for a Mirnov coil in the case of AUG#30815 at 2.97s (sawtooth D). A small precursor activity is measured with a fixed frequency. Right: (same sawtooth) radial displacement of the core ξ as obtained from the SXR measurements (dash-dotted red line) compared with simulation of tungsten (radial position of maximum of density in black and magnetic core in green).

as the sum of the sawtooth field and a centrifugal contribution:

$$\mathbf{E} = \mathbf{E_{sth}} + \mathbf{E_c} \quad \text{where} \quad \mathbf{E_{sth}} = -\boldsymbol{\nabla}\Phi + \frac{\dot{\psi}_*}{R}\mathbf{e}_\varphi \quad ; \quad \mathbf{E_c} = \frac{m}{Z_i e} R\Omega^2 \mathbf{e_R} \ . \tag{6}$$

This results in the following equation for the total energy evolution:

$$\frac{\mathrm{d}\mathcal{E}}{\mathrm{d}t} = (Z_i e)\left[\frac{v_\varphi}{R}\left(\frac{\partial\psi}{\partial t}\right) + \left(\frac{\partial\Phi}{\partial t}\right)\right] + \mathbf{f_c}\cdot\mathbf{v} \ . \tag{7}$$

Furthermore, to avoid the creation of a large population of tungsten ions that have a kinetic energy equal to zero, we arbitrarily limit the minimum value of the kinetic energy to 1keV during the simulations, mimicking the effect of the collisions.

3.2. Dynamics of the maximum of emission

The Soft X-Ray (SXR) diagnostics at ASDEX Upgrade consist of several pinhole cameras [16] gathering 208 lines of sight lying in a poloidal plane at a given toroidal position. The diode currents are originally recorded at sample rates of 500 kHz or 2MHz, allowing a time resolution of about 2μs and a good coverage of fast MHD phenomenona. The cameras further allow tomographic reconstruction of the plasma SXR emission [17].

The plasma of ASDEX Upgrade contains a significant amount of tungsten impurity because it is the main material of most plasma facing components. The emission of SXR can thus be in first approximation related to the line-radiation emission of tungsten and considered proportional to the density of tungsten in the plasma [18].

The approximate description of the tungsten distribution is used in EBdyna to give a qualitative interpretation of the Soft X-Ray measurements obtained during the sawteeth considered in terms of radial displacement of the core ξ. An illustration is given in figures 3 and 4 (for sawteeth D and B) where it is seen that the complete reconnection model can account for the measured emission. The oscillations of the signal in radial position are qualitatively explained by the phase with the mode rotation and the effect of the centrifugal force on the impurity ions.

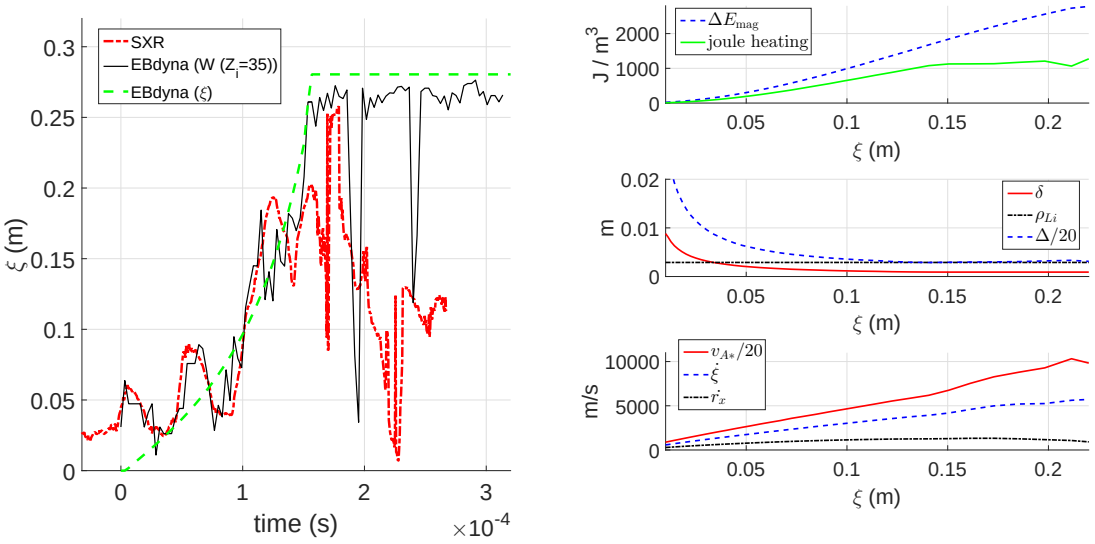

Figure 4. Left: radial displacement of the core ξ as obtained from the SXR measurements (dash-dotted red line) for AUG#30382 at 2.5s (sawtooth B). Also plotted is the simulation of tungsten (radial position of maximum of density in black and magnetic core in green dashed). The crash duration in the simulation was extended to 150μs to account for the precursor phase (initial measured value of ξ of about 4cm reached after roughly 30μs in the simulation). Right: evolution of the main parameters (sawtooth B) involved in equation (8) as a function of the displaced position of the core ξ. In the top plot, the difference between ΔE_{mag} and joule heating is the energy density converted into the outflow kinetic energy in the layer (v_{A*}). This in turns yield a given value of $\dot{\xi}$ and the calculation gives a crash time of 117μs. In the middle plot, we can notice that the value of the layer width δ becomes smaller than the ion Larmor radius ρ_{Li} only when ξ esceeds a few centimeters, which can be understood as indicating a change in the kink regime for a small threshold value of displacement. This could subsequently explain the reconnection phase when the kink exceeds a small threshold precursor displacement.

However, although it accounts qualitatively for the measured SXR emission, there is an open discussion as to the validity of a complete reconnection modelling where the core is moving from $\xi = 0$ to $\xi = r_{\mathrm{mix}}$. Experimentally, in ASDEX Upgrade, there is evidence of precursor activity from SXR measurements that show an exponentially slowly growing trend for the radial displacement of the core up to a small value ($\sim 0.08a$). This phenomenon can be related to the $m = 1$ mode. Thus the core is initially displaced of a few centimeters before the reconnection begins. This initial displacement can be

compensated in the modelling by allowing a bit more time for the reconnection phase in the simulation than what is actually measured (see for example figure 4).

Furthermore, plasma parameters such as the diamagnetic frequencies at the reconnection site [19] suggest that the reconnection might be incomplete (see section 3.4). However, there is no way to discriminate the completeness of the reconnection by solely using the SXR signals. An incomplete reconnection pattern can be mimicked by the modelling by interrupting the simulation before ξ has reached $r_{\rm mix}$.

To summarize this subsection, the measured SXR redistribution patterns of the impurity ions are close to those obtained with a Kadomtsev-like complete-reconnection description as implemented in EBdyna and applied to impurity ions (see for example figures 3 (right) and 4 (left)) The real phenomenon is certainly actually very complex: a precursor is certainly visible in all crashes and uncertainty remains as to the degree of completeness of the reconnection. Additional modelling related to stochastization of the field lines [20] could also be investigated. We can only assess that our representation accounts for the redistribution of the ions.

3.3. Complete reconnection estimate of the crash duration τ_{cr}

Simulations do not account for the remaining perturbed signal as seen by Mirnov coils (eg. figure 3, left where one can notice an $n = 1$ perturbation remaining for about 20ms after the crash). This feature possibly indicates an incomplete reconnection or the presence of runaway electrons (localized current) or MHD modes after the crash. However, in first approximation, the complete reconnection model can be further analyzed in terms of the dissipation of magnetic energy during the reconnection: in particular we do so to get a numerical estimate of the sawtooth crash duration according to the background plasma parameters. A simple geometrical analysis yields, according to mass conservation:

$$\dot{\xi}\Delta = 2v_{A*}\delta \tag{8}$$

where v_{A*} is the outflow velocity, δ is the radial layer width and Δ is the approximate length of the reconnection region in the poloidal plane. At one instant in time, the plasma volume $\delta\mathcal{V}_1$ enters the layer with the helicity B_{*1} from the core and the volume $\delta\mathcal{V}_2$ with B_{*2} enters from the outer region. The plasma of mass density $m_i n_i$ then leaves the layer with the helicity B_{*3}. The approximate values of the fields are those obtained in the pre- and post-sawtooth configurations by using the the circular approximation $B_* = B_{\rm pol}(1-q)$ (and using the Kadomtsev post-sawtooth values of q to estimate B_{*3}). The energy entering the reconnection region per unit time is mostly magnetic. The difference of magnetic pressure $\Delta P_{\rm mag}$ between the inflow and the outflow has to be reflected by an increase of the kinetic energy of the plasma or be dissipated through Joule heating inside the layer through the term $\Delta\mathcal{E}_\eta$. The overall energy density balance in the layer is thus approximately:

$$\Delta P_{\rm layer} = \Delta P_{\rm mag} - \frac{\Delta\mathcal{E}_\eta}{\delta\mathcal{V}_3} \simeq \frac{1}{2\mu_0}\left(\frac{B_{*1}^2 + B_{*2}^2}{2} - B_{*3}^2\right) - \frac{\Delta\mathcal{E}_\eta}{\delta\mathcal{V}_3} = \frac{1}{2}m_i n_i v_{A*}^2 \tag{9}$$

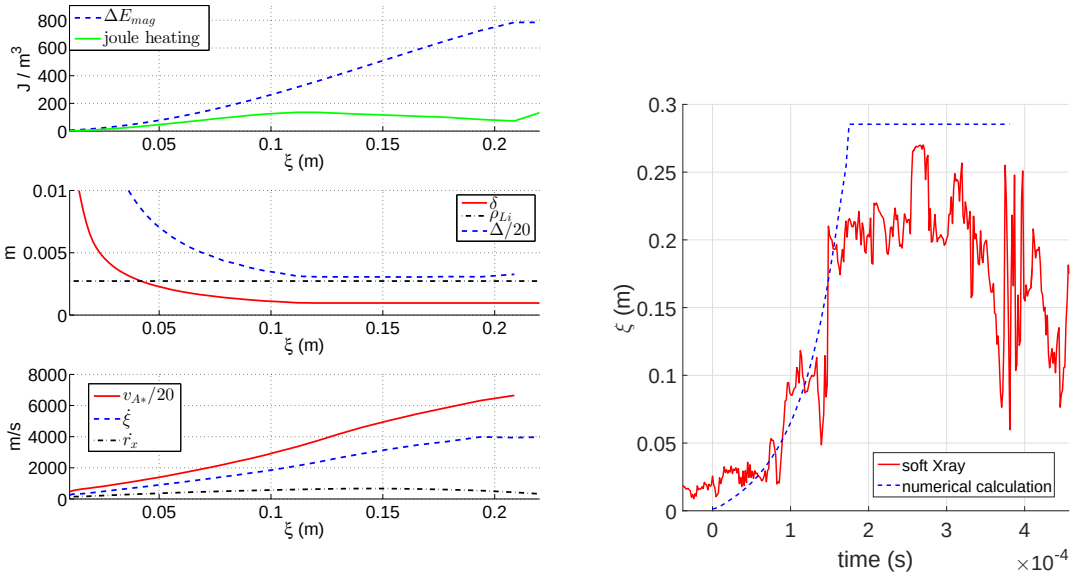

Figure 5. Experimental case of the ASDEX Upgrade discharge #31557 (crash at 2.25s), sawtooth E. Left figure: evolution of the main parameters involved in equation (8) as a function of the displaced position of the core ξ. Right figure: Compared evolution of the average radial position of the core (ξ). One curve is from experimental measurements (soft Xray in red, full line) and one from the modeling as implemented in EBdyna (dashed blue line). The calculation gives a crash time of 180μs. The mode might be in drift-tearing regime at this time.

where $\delta\mathcal{V}_3$ corresponds to the global volume of plasma transiting through the layer during the time interval dt and we have considered $\delta\mathcal{V}_1 \sim \delta\mathcal{V}_2 \sim \delta\mathcal{V}_3/2$; the losses through Joule heating are expressed as: $\Delta\mathcal{E}_\eta = \eta_\parallel \tilde{j_\parallel}^2 \mathcal{V}_{\rm layer}$ with $|\tilde{j_\parallel}| \simeq (|B_{*1} - B_{*3}|)/(2\mu_0\delta)$ and $\mathcal{V}_{\rm layer} = 2\pi R_0 \delta d_e$. It is possible to use an extended Ohm's law to estimate the width of the layer δ. Following the interpretation given in [21], we consider:

$$\delta \simeq \; d_e \left(\frac{1}{\tau_{A*}} + (1-q_0)\frac{v_{\rm the}}{R} \right)^{1/2} \tau_{A*}^{1/2} \quad \text{with} \quad v_{\rm the} = \sqrt{\frac{2T_e}{m_e}} \tag{10}$$

and we retain for the transit time of the ions in the layer the expression $\tau_{A*} = \Delta/v_{A*}$. A simple numerical solver is designed trying different dynamics for τ_{cr} in order to minimize the difference between the LHS and the RHS in (8), using the values given by (9) and (10). We are using as an initial guess the dynamics for ξ introduced in [4] when a linear evolution of the shaping parameter α with time is considered. The solver converges to similar values ('τ_{cr} reco' values given in table 1) of τ_{cr} as that observed experimentally (τ_{cr} exp), provided Joule dissipation or plasma toroidal rotation do not become dominant. An illustration is given in figures 4 and 5. However, the relatively large resistivity in the considered ASDEX Upgrade experiments makes the overall model subjective. We again recall that the model we have given in this section only gives us a qualitative reference (allowing for extrapolation to larger experimental devices).

3.4. Partial reconnection

Experimentally, some measurements indicate that the reconnection is often incomplete [22] in ASDEX Upgrade typical discharges. A possible explanation for this phenomenon was sought in [23] and can be interpreted in a tokamak plasma in terms of competition of diamagnetic and Alfvén dynamics [19]. It suggests that the reconnection is halted when the following criterion is satisfied:

$$v_{ie*} = |\mathbf{v}_{*\mathbf{i}} - \mathbf{v}_{*\mathbf{e}}| > v_{A*} \tag{11}$$

where v_{A*} is the outflow velocity from the reconnection point as described previously (equation (9)) and $\mathbf{v}_{*\alpha} = -(\boldsymbol{\nabla} P_\alpha \times \mathbf{B})/(Z_\alpha e n_\alpha B^2)$ are the radial diamagnetic velocities measured at the exit of the reconnection site for species $\alpha = i, e$. Quantitatively, we can in first instance combine the ion and electron contributions and use our model to evaluate the gradient of electron pressure $\nabla P_e = (P_{e(\text{core})} - P_{e(\text{island})})/(\Delta/2)$. The most likely candidates for partial reconnection are then cases C and E, that correspond to large sawteeth with low values of $|q-1|$ in the core region, yielding a low amount of magnetic energy dissipation. In particular, calculations of (11) in the case E hint to a slightly incompletely reconnected magnetic core. Numerically, the amount of redistribution of ions can be evaluated by simply interrupting the simulation before the core has reached the mixing radius position. We remind here that the measurement of the safety factor inside the experimental device is not always obtained with a good precision, and that this contributes to our lack of knowledge of the behaviour of plasma in the post crash phase (see for example figure 10).

4. Redistribution of Neutral Beam ions compared with the measurements

4.1. Collective Thomson Scattering (CTS) measurements

CTS offers the capability to measure the fast ion distribution locally. As it propagates through the plasma, the radiation from a high power probe beam 'scatters off' plasma fluctuations. The received signal bears a signature of the ion velocity distribution (due to Doppler shift of the signal) provided that the scattering is dominated by collective effects. If we denote λ_D the Debye length, this requires that $|\lambda_D \mathbf{k}_\delta| < 1$. Here the resolved fluctuation wave vector is defined as $\mathbf{k}_\delta = \mathbf{k_s} - \mathbf{k_i}$, where i and s refer to the incident and scattered wave vectors, respectively. A frequency shift in scattered radiation ν_δ can be approximately related to an ion velocity $\mathbf{v_{ion}}$ by $\nu_\delta = \nu_s - \nu_i = \mathbf{v_{ion}} \cdot \mathbf{k}_\delta / 2\pi$.

In ASDEX Upgrade the incident diagnostic probe beam is created by a gyrotron with an output frequency of 105 GHz and typical output power of 500 kW [24]. A forward model of the emission based on available measurements of the bulk plasma parameters and the fast-ion distribution function from TRANSP or EBdyna_go can be obtained. The overall reconstructed emission (adding reconstructed NBI and thermal emission) closely match the measured ones (figure 6: dashed lines matching the error bars). Further interpretation of the spectra in terms of distribution of velocities can be

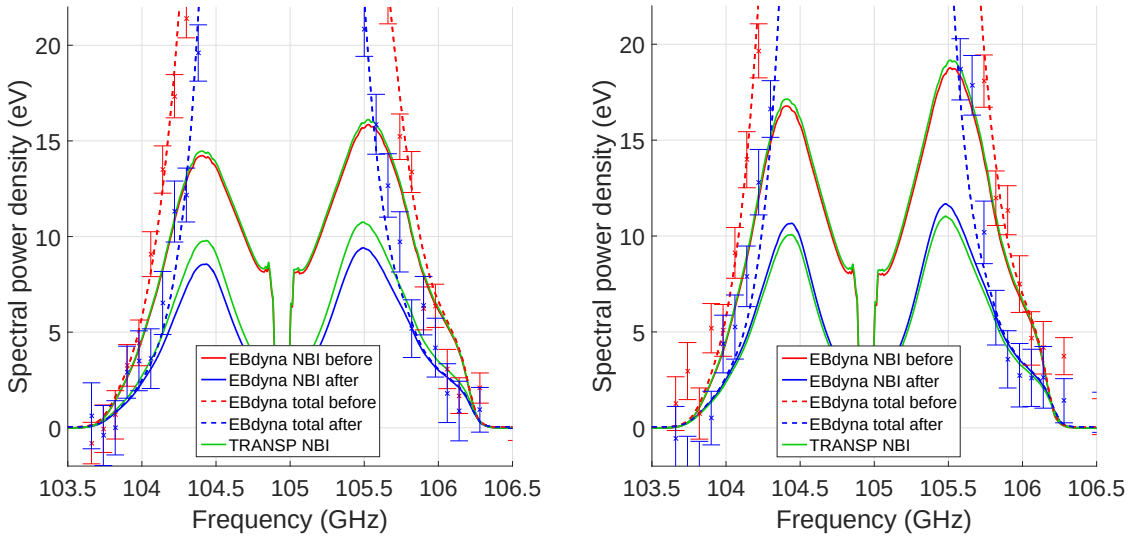

Figure 6. Illustration of the CTS spectrum obtained from the measurements (error bars). The red plots correspond to the ion measurements and simulations before the crash, the blue ones to the post-sawtooth configuration. The green line correspond to TRANSP data. The full lines correspond to the reconstructed emission from the simulated NBI, the dashed lines ot the total emission (including background contribution). The total intensity (dashed lines) as obtained from EBdyna simulations can be compared with a reconstructed emission based on the NBI simulation and measured thermal-ion plasma properties for the case of the crash AUG#30382 at 2.3s (left) and AUG#30382 at 2.5s (right).

obtained by fitting the spectra with a scattering model within a Bayesian framework. Ultimately, the CTS measurements could complement the FIDA ones [25].

4.2. Fast Ions Deuterium-Alpha (FIDA) spectroscopic measurements

The FIDA diagnostic technique is Charge-eXchange Recombination Spectroscopy (CXRS) applied to fast D-ions: it uses the Balmer alpha emission line [7] with a time resolution of 2ms.

We can compare reconstructed signals from two different views with the measured intensity as it is done in figure 7. Good agreement is found for AUG#30382 at 2.5s where the remaining discrepancy can be explained by the absence of a source term (NBI fueling) in EBdyna. The FIDA diagnostic can further be used as a tomographic system ([27],[28]) aimed at resolving the velocity space of fast Deuterium in the experiment [29]. The tomographic inversion of the FIDA measurements allows us to calculate the redistribution of fast particles resolved in velocity space. In particular, we evaluate the relative change of density before ($_{ini}$) and after the crash ($_{end}$). We thus measure $-(\Delta n)/n_{ini} = -(n_{end} - n_{ini})/n_{ini}$ as it is shown in figure 9. Since the NBI is injected along the direction of the current, the tomographic inversion for negative pitch ($\mathcal{P} < -0.2$) has large uncertainties [30]. The measured part of the distribution for these

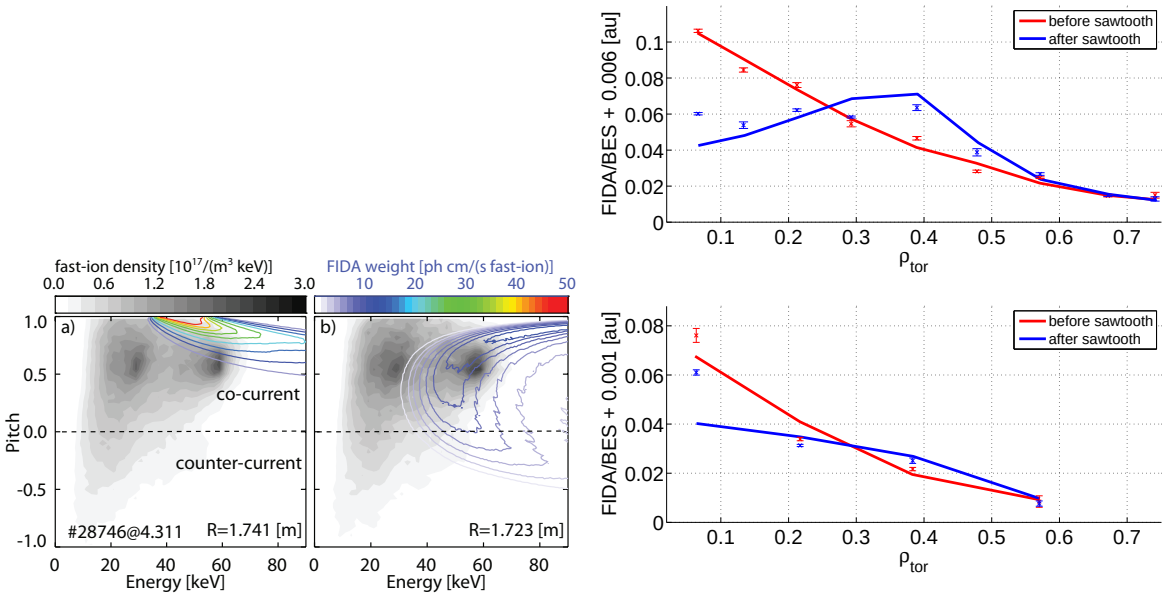

Figure 7. Left: velocity space coverage of two of the FIDA lines of sight (left: toroidal view; right: poloidal view) at two particular Doppler shifts ([26] and [27]). Right: illustration for AUG#30382 at 2.5s (sawtooth B) of the reconstructed FIDA signal normalized to the beam signal (BES). An arbitrary offset is used to account for background emission. The error bars are the experimental signals, the full lines are reconstructed emissions from the simulations. Top plot: toroidal view; bottom plot: poloidal view.

values of pitch is not reliable, especially at high energies.

The TRANSP data was actually generated so that the distribution of particles was in the laboratory frame of reference, so that the parallel velocities $v_{\parallel_{\mathrm{TRANSP}}}$ include the toroidal rotation in the distribution. Our simulations, however, consider the magnetic perturbation in the plasma frame. To obtain a representation of the particles in the frame of reference of the bulk of the plasma, we thus need to use in the simulation a fictitious parallel velocity $v_{\parallel_{\mathrm{EB}}}$ and modify the initial (^{ini}) and final (^{end}) values of velocities and energies of each particle. The simulations including toroidal rotation are thus done with the following approximate corrections, considering in first approximation that the toroidal rotation of a given particle $\Omega_i = \Omega(\psi)_{ini}$ affects mostly the parallel velocity of the particles:

$$\begin{aligned} v^{ini}_{\parallel_{\mathrm{EB}}} &= v^{ini}_{\parallel_{\mathrm{TRANSP}}} - R\Omega_i \\ v^{end}_{\parallel_{\mathrm{sim}}} &= v^{end}_{\parallel_{\mathrm{EB}}} + R\Omega_i \end{aligned} \tag{12}$$

where $v^{end}_{\parallel_{\mathrm{sim}}}$ corresponds to the final value used to compare with the measurements. Expressions (12) correspond to a correction on the complete NBI distribution. The kinetic energy also needs to be recalculated accordingly, by keeping the perpendicular part constant.

The tomography reconstruction is studied in the case of AUG#31557 at 2.25s

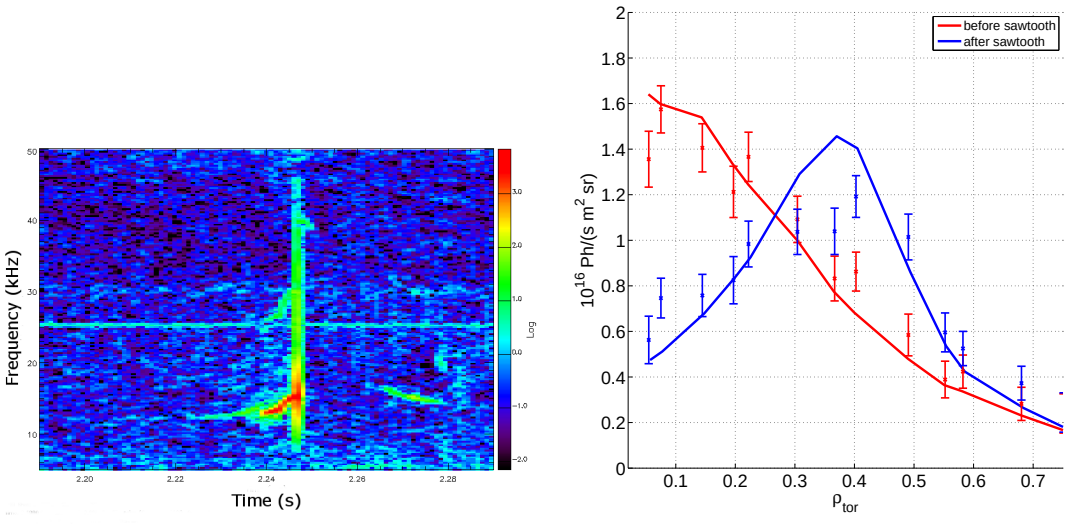

Figure 8. Left: Spectrogram from a Mirnov coil signal for the crash AUG#31557 at 2.25s (sawtooth E). A significant precursor activity is seen at about 12kHz before the sawtooth (main vertical line). The mode might be in drift-tearing regime at this time. Right: toroidal view of FIDA for the same sawtooth. The error bars are the experimental signals, the full lines are reconstructed emissions from the simulations. The signal is here represented in absolute magnitude.

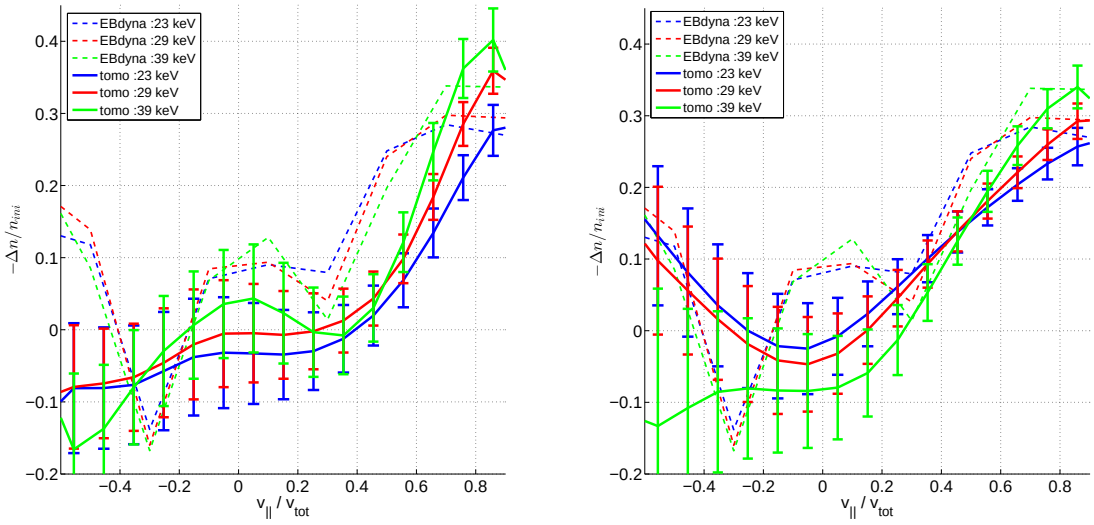

Figure 9. Relative change of density during the sawtooth according to pitch. The considered poloidal positions were around $\rho_{tor} \sim 0.27$. We compare the EBdyna simulations with FIDA tomography for the crash AUG#31557 at 2.25s (sawtooth E). The crash duration in the simulation was about 155μs. Left: simulation compared with the Minimum Fischer [30] tomography method. Right: simulation compared with the first order Tikhonov tomography method. The latter yields a better agreement with our modelling.

with two different tomography reconstruction methods described in [30]. The Minimum Fischer method retains a feature around $\mathcal{P} \simeq 0$ that is present also in the simulations. It is however qualitatively a bit different for positive values of pitch. On the other hand, a good agreement is obtained at postive values of pitch with the method of first order Tikhonov. This is shown in figure 9, giving confidence both in the tomography values and in the relevance of the simulation model. In particular the trend of the amount of redistribution of the passing particles with energy and pitch is measured by the first order Tikhonov method and recovered in the simulation.

5. Insights into the dynamics of the NBI fast ions during a sawtooth

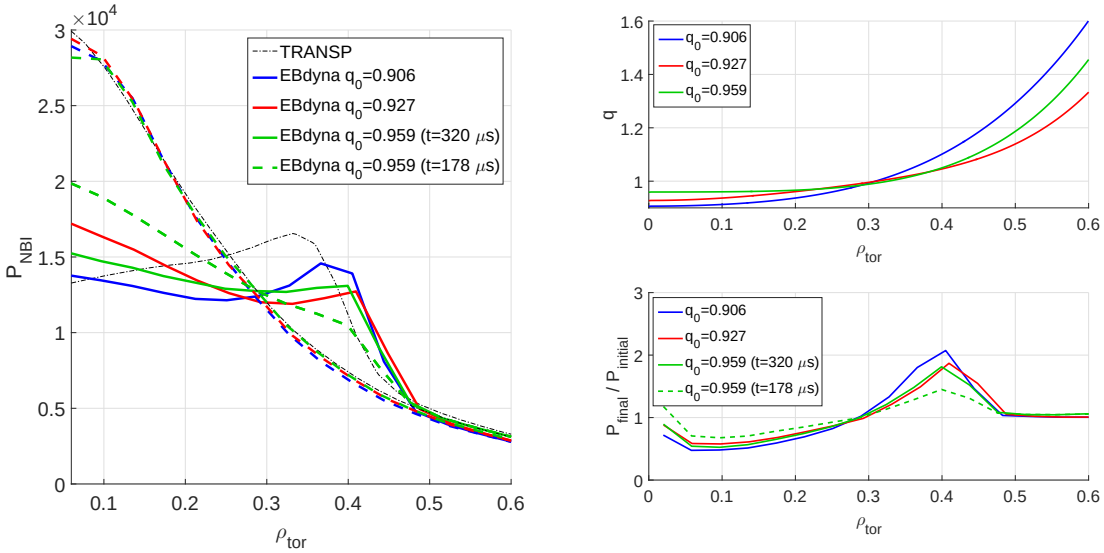

Figure 10. Compared redistribution of the total NBI pressure $P_{\rm NBI}$ for different safety factor profiles, representative of the experimental case AUG #32324 at 2.46s (sawtooth C). Left: The TRANSP prediction is compared with different EBdyna simulations. The case $q_0 = 0.906$ was treated with a crash duration of about $115\mu s$. The cases $q_0 = 0.927$ and $q_0 = 0.959$ were treated with a crash duration of about $155\mu s$. The case $q_0 = 0.959$ was treated at two separate time points: just after the end of the reconnection ($t = 178\mu s$) and at the end of the simulation ($t = 320\mu s$). Right figure: EBdyna simulations corresponding to the profiles from the left figure. Top figure: safety factor profiles in the EBdyna simulations, before the sawtooth. Bottom: relative change of pressure with different on-axis safety factor profile values q_0. The first time point is more representative of the FIDA measurements.

As was shown in [2], for an ion of mass m and charge $Z_i e$:

$$\frac{\mathrm{d}}{\mathrm{d}t}(Rm\mathrm{v}_\varphi - (Z_i e)\psi) = -(Z_i e)\left[\frac{\partial \Phi}{\partial \varphi} + \frac{v_\varphi}{R}\frac{\partial \psi}{\partial \varphi}\right] . \tag{13}$$

We may note that a consequence of this result is that, in an axi-symmetric configuration, the quantity on the LHS of equation (13), $p_\varphi = Rm\mathrm{v}_\varphi - (Z_i e)\psi$ is conserved. p_φ is the

toroidal canonical angular momentum that we can use as an estimate of the average flux surface position of a fast particle with given pitch and energy.

5.1. Global NBI pressure redistribution as a function of $|q-1|$ in the core region

In order to give an idea of the importance of the safety factor profile on the redistribution, we have plotted in figure 10 the TRANSP prediction compared with EBdyna simulations considering different radial safety factor profiles. When the on-axis safety factor profile value gets closer to unity, the amount of magnetic energy available during the reconnection is significantly reduced, and this yields a slower reconnection process. However, the case with the flattest q profile in the core region yields a peculiar behaviour of the ions during the second phase of the collapse. The redistribution seems to be enhanced during this phase by this specific configuration, unlike in the other case where its impact is unimportant. Indeed, the pattern obtained at the end of the reconnection phase ($t = 178\mu s$) is closer to the measurements. This means that, when the complete reorganization phase is included in the sawtooth description in EBdyna on time scales similar to the reconnection phase, it actually yields a simulation result that is further away from the measured amount of redistribution of fast ions when this phase is omitted. Thus the existence, inside the experiment, of the reorganization phase after reconnection in the case of safety factor close to unity is questionable. It could also be that the reorganization occurs on much longer time scales ($> \tau_{\rm cr}$) than what was prescribed in the simulation.

5.2. Behaviour of trapped energetic ions

The trapped fast D particles represent in these experiments about 30% of the global NBI population. An important result of the previous work of Kolesnichenko et al. [4] is that, when equaling the crash time with the drift precession period, there is evidence of an energy threshold above which more than half of the energetic trapped ions is not redistributed by the sawtooth and is effectively detached from the reconnecting field line motion of the sawtooth crash. It scales as

$$\mathcal{E}_{crit} \simeq r_1 R_0 (Z_i e) B_0 \omega_{cr} \quad \text{with} \quad \omega_{cr} \sim 1.5\pi/\tau_{cr} \ . \tag{14}$$

We thus find the approximate scaling $\mathcal{E}_{crit} \simeq 4/\tau_{cr}$ in eV in the considered experiments. This roughly corresponds to the range $30-40$keV for Deuterium ions in our simulations. This is illustrated in figure 11 for the NBI trapped population that was initially in the core.

Actually, the situation is made more complicated by the presence of a resonant [2] pitch (specific value of λ_0): a small fraction of the trapped population is not able to circulate in the helicity of the crash (precession $\omega_{vD} \sim 0$) and thus remains attached to it up to higher energies. This feature partly explains the lesser effect of the crash dynamics in figure 11 compared with what would be expected from expression (14): for example, if we look at a redistribution of trapped particles of 0.3 of the thermal value,

one get the values of $\mathcal{E}_{\text{crit}}$ as 26keV, 38keV and 55keV instead of the expected 19keV, 38keV and 76keV from (14).

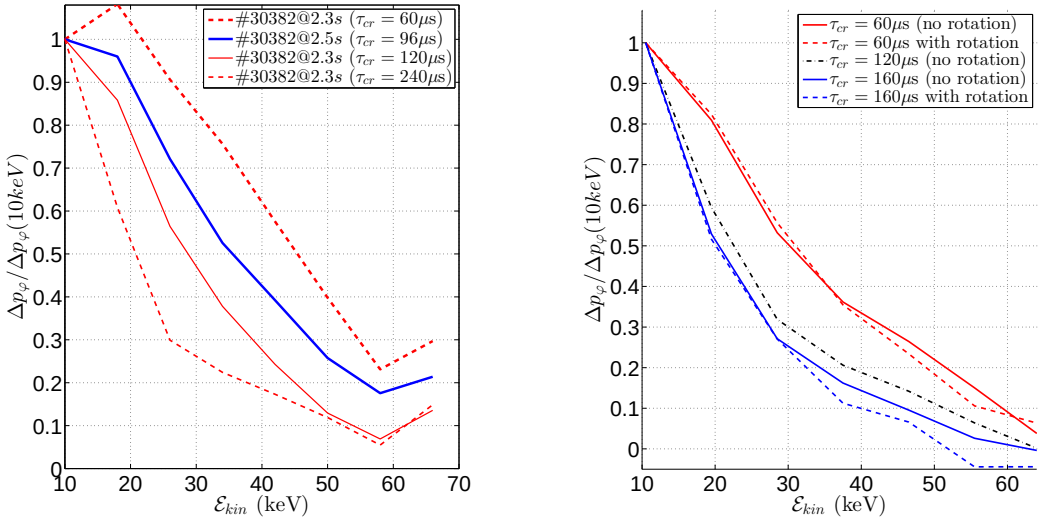

Figure 11. Relative redistribution (change of flux surface normalized to the 10keV value) of trapped fast NBI particles. Left: sawtooth A and B, several dynamics yielding various values of $\mathcal{E}_{crit}$ (Δp_φ refers to the change of p_φ, and thus of radial position, during the sawtooth). Right: sawtooth D, three dynamics. The redistribution for the crash times $\tau_{cr} \sim 60\mu s$ and $\tau_{cr} \sim 160\mu s$ were calculated without and with toroidal rotation effect. No significant impact on the redistribution of the trapped population is observed.

5.3. Behaviour of passing energetic ions

The co-current circulating fast D particles represent about 58% of the global NBI population. The circulating particles have their behaviour mostly guided by the value of their pitch $\mathcal{P}$ or correspondingly their trapping parameter λ_0. As was studied in [2], there is qualitatively an impact of the orbit width δ_r of the particles on their interaction with the perturbation. In particular, increasing kinetic energy will increase δ_r and this will enhance the radial $\mathbf{E} \times \mathbf{B}$ drift felt by the ions.

Barely circulating ions have different trends of increased or decreased redistribution as a function of kinetic energy. It is due to the increase of the ratio between drift precession ω_{vD} and longitudinal precession ω_ψ allowing partial detachment [2]. Values of ω_{vD}/ω_ψ greater than one (as observed for barely passing ions) will change the trend from increased redistribution to increased detachment : the passing ions then behave like the trapped particles. This is shown in figure 12 and is qualitatively recovered for extreme pitch values ($\mathcal{P} \sim 0.2$ and $\mathcal{P} \sim 1$) by the tomography (figure 9, right).

In particular, in figure 12, the comparison of two different safety factor profiles (top plots, $q_0 = 0.86$ (left) and $q_0 = 0.65$ (right)) yield different value of longitudinal precession $\omega_\psi \simeq \left\langle v_\parallel (q-1) \right\rangle / R_0$. The average should be considered over one particle

orbit. The lower q_0, the higher ω_ψ tends to be for the fast particles. This is seen to have a significant impact on the amount of barely passing particles ($\mathcal{P} \sim 0.25$) that are redistributed. Comparing top left and bottom left plots in figure 12, we can see that the effect of toroidal rotation is to decrease slightly the effective pitch of the particles in the plasma frame. The ions thus tend to be less redistributed when rotation is considered, even at higher pitch.

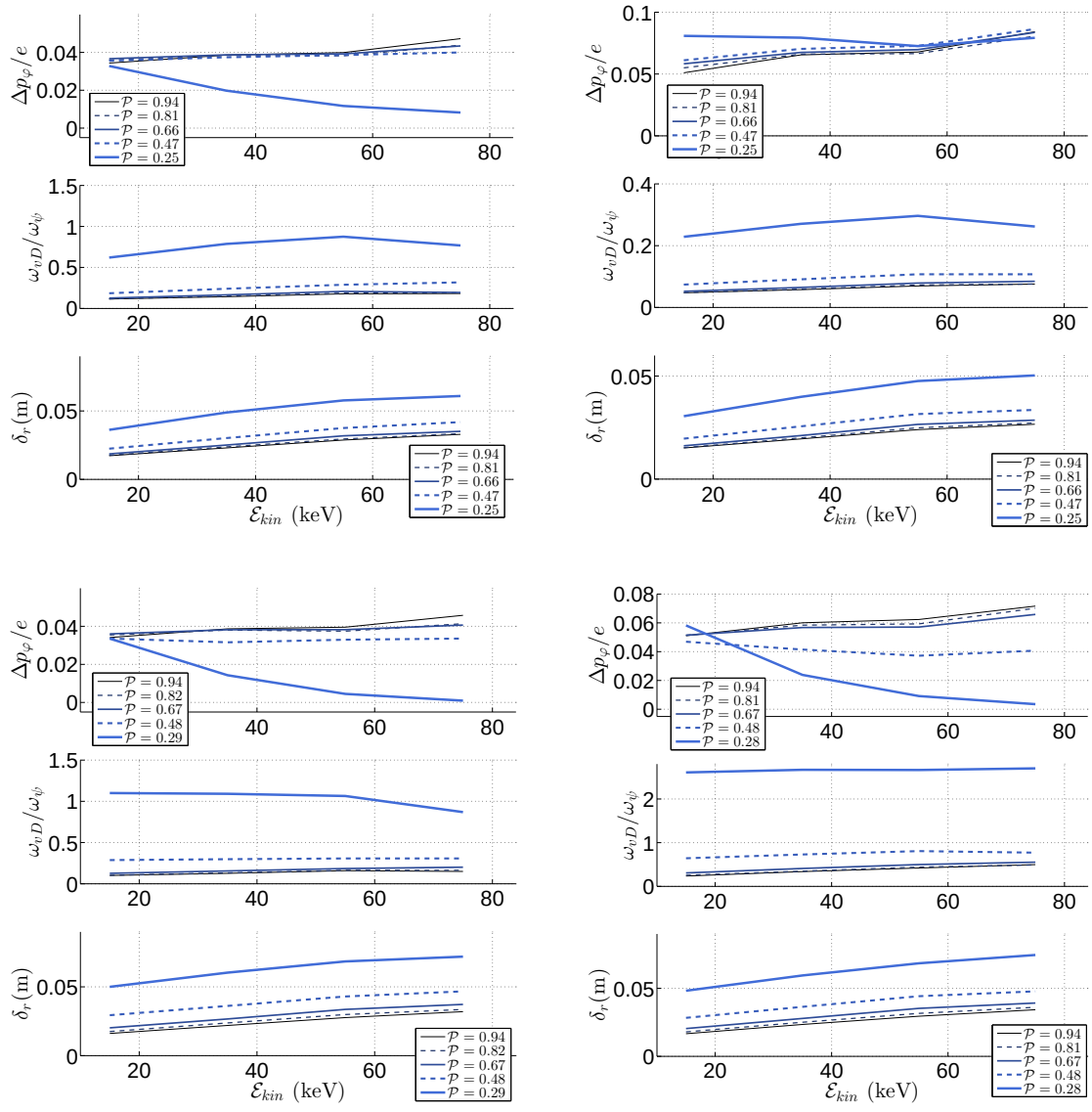

Figure 12. Illustration of the influence of pitch and energy of co-current passing particles (in the core region $q < 0.97$). The crash duration considered was $\tau_{cr} \sim 120\mu$s. Top left: the crash AUG#30815 at 2.97s (case D $q_0 \sim 0.86$) without rotation. Top right: the crash AUG#30382 at 2.3s (case A $q_0 \sim 0.65$) without rotation. Bottom left: the crash AUG#30815 at 2.97s (case D) with rotation. Bottom right: the crash AUG#31557 at 2.25s (case E $q_0 \sim 0.962$) with rotation.

6. Conclusions

We have implemented a numerical model of the ASDEX Upgrade tokamak in EBdyna_go in order to simulate the effect of a sawtooth collapse on a population of tungsten impurities and one of high energy ions from NBI. We have successfully reconstructed various sawtooth crashes according to ASDEX Upgrade experiments. The code assumes complete reconnection. Uncertainty remains on the actual degree of reconnection of the core after the crash; $|q-1|$ is also a free parameter, not well determined from the experiment: these two unknowns cannot be eliminated simultaneously by matching the experimental data and hence there should be further studies to investigate various post-crash configurations, both with simulation and measurements.

An additional simple tool was developed to estimate the crash duration according to the reconnected magnetic energy. The comparison of the evolution of the maximum of emission according to SXR tomography and maximum of density of tungsten impurity simulations show good agreement. NBI fast particle simulations yield good qualitative agreement between simulations and FIDA or CTS measurements. The matching is improved when toroidal rotation is introduced: the trend of redistribution with the pitch profiles and kinetic energy as obtained with the FIDA tomography is recovered. Future work will address the refinement of the modelling and its use to investigate the fast ion losses and the impact of pre-sawtooth and post-sawtooth MHD activity in various background plasma conditions.

Acknowedgements

This work has been carried out within the framework of the EUROfusion Consortium and has received funding from the Euratom research and training programme 2014-2018 under grant agreement No 633053. The views and opinions expressed herein do not necessarily reflect those of the European Commission.

References

[1] van Goeler S., Stodiek W. and Sauthoff N. 1974 *Physical Review Letters* **33** 1201
[2] Jaulmes F., Westerhof E. and de Blank H.J. 2014 *Nucl. Fusion* **54** 104013
[3] Kadomtsev B. B. 1975 *Sov. J. Plasma Phys.* **1** 389
[4] Kolesnichenko Ya. I. and Yakovenko Yu. V. 1996 *Nucl. Fusion* **36** 159
[5] Pankin A. et al. 2003 *Computer Physics Communications* **159** 157
[6] Nielsen S.K. et al. 2015 *Plasma Phys. Control. Fusion* **57** 035009
[7] Geiger B. et al. 2011 *Plasma Phys. Control. Fusion* **53** 065010
[8] Chapman I. et al. 2011 *Plasma Phys. Control. Fusion* **53** 124003
[9] Beliën A.J.C. et al. 2002 *Journal of Computational Physics* **182** 91
[10] Bussac M.N. et al. 1975 *Physical Review Letters* **35** 1638
[11] Porcelli F., Boucher D., and Rosenbluth M. N. 1996 *Plasma Phys. Control. Fusion* **38** 2163
[12] Porcelli F. 1991 *Physical Review Letters* **66** 425
[13] Pegoraro F. et al. 1989 *Phys. Fluids B* **1** 368
[14] Keppens R. and Blokland J.W.S. 2006 *Fusion Sc. and Technol.* **49** 131

[15] Pütterich T. et al. 2010 *Nucl. Fusion* **50** 025012
[16] Igochine V. et al. 2010, *Soft X-ray Diagnostic on ASDEX Upgrade*, **IPP 1/338** Zitierlink: http://hdl.handle.net/11858/00-001M-0000-0026-F036-B
[17] Bessenrodt-Weberpals M. et al. 1996 *Plasma Phys. Control. Fusion* **38** 1543
[18] Weiland M. et al. 2015 *Plasma Phys. Control. Fusion* **57** 085002
[19] Beidler M.T. et al. 2011 *Physical Review Letters* **107** 255002
[20] Igochine V. et al. 2010, *Phys. Plasmas* **17** 122506
[21] Wesson J. 2004, *Tokamaks 3rd edition*, Oxford Science Publications
[22] Letsch A. et al. 2002 *Nucl. Fusion* **42** 1055
[23] Swisdak M. et al. 2003 *Journal of Geophysical Research* **108** 1218
[24] Rasmussen J. et al. 2015 *Plasma Phys. Control. Fusion* **57** 075014
[25] Salewski M. et al. 2010 *Nucl. Fusion* **50** 035012
[26] Geiger B. et al. 2014 *Nucl. Fusion* **54** 022005
[27] Salewski M. et al. 2014 *Plasma Phys. Control. Fusion* **56** 105005
[28] Salewski M. et al. 2014 *Nucl. Fusion* **54** 023005
[29] Geiger B. et al. 2015 *Nucl. Fusion* **55** 083001
[30] Jacobsen A.S. et al. 2015, *Plasma Phys. Control. Fusion* Inversion methods for fast-ion velocity-space tomography in fusion plasmas, submitted